Monthly Notices
of the
ROYAL ASTRONOMICAL SOCIETY

MNRAS **433,** 3290–3296 (2013)
Advance Access publication 2013 June 21

doi:10.1093/mnras/stt969

Searching for the missing iron mass in the core of the Centaurus cluster

E. K. Panagoulia,[1]★ A. C. Fabian[1] and J. S. Sanders[2]

[1]*Institute of Astronomy, Madingley Road, Cambridge CB3 0HA, UK*
[2]*Max-Planck-Institute für extraterrestrische Physik, D-85748 Garching, Germany*

Accepted 2013 June 1. Received 2013 May 14; in original form 2013 January 31

ABSTRACT

We re-analyse a combined 198 ks *Chandra* observation of NGC 4696, the brightest galaxy of the Centaurus cluster. We extract temperature and metallicity profiles from the data, and we confirm the presence of a sharp drop in iron abundance, from ∼1.8 to ∼0.4 $Z_{\odot}$, within the central 5 kpc of the cluster. We estimate that this central abundance drop corresponds to a total 'missing' iron mass of 1.4×10^6 $M_{\odot}$. We propose that part of this missing iron is locked up in cool (∼19 K), far-infrared emitting dust, as found by *Spitzer* and *Herschel* observations. This can occur if the iron injected by stellar mass-loss in the central region is in grains, which remain in that form as the injected dusty cold gas mixes and joins the cold dusty filamentary nebula observed within the same region. The bubbling feedback process observed in the cluster core then drags filaments outward and dumps them at 10–20 kpc radius, where the metallicity is high.

Key words: galaxies: clusters: general – galaxies: clusters: individual: Centaurus – galaxies: individual: NGC4696.

1 INTRODUCTION

Galaxy clusters are the brightest extended X-ray sources in the Universe. The intracluster medium (ICM) is observed in the X-ray through the emission of thermal bremsstrahlung radiation and line emission, as it is gravitationally compressed and heated to temperatures of 10^7–10^8 K. Spectroscopic studies of the ICM have shown that it is enriched with metals expelled from the cluster galaxies, while an average background metallicity of ∼0.3 solar has also been observed (e.g. Edge & Stewart 1991). By comparing the ICM metallicity profiles with those produced by supernova (SN) simulations, it was proposed that this background enrichment is due to SNe, which occurred early in the life of the cluster (Finoguenov, David & Ponman 2000; Loewenstein 2006; de Plaa et al. 2007).

Previous studies of galaxy clusters have allowed us to distinguish two different types of clusters, on the basis of their surface brightness profile. The first type are the clusters which show a sharp surface brightness peak towards the centre; these are cool-core (CC) clusters. Non-CC clusters do not show such a surface brightness peak. CC clusters display little recent merger activity, and are believed to be dynamically relaxed. The ICM cooling time in these CC clusters is often much shorter than the age of the cluster itself. Hence, according to the cooling flow model (for a detailed description, see Fabian 1994), large amounts of cold gas and star formation are expected to be found at the cores of these clusters. However, detailed X-ray observations of these clusters have shown that the amount of gas, with a temperature 2 to 3 times lower than the ambient gas, is much smaller than expected from the cooling flow model (Peterson & Fabian 2006; McNamara & Nulsen 2007, 2012). In addition, the cooling flow model severely overpredicts the star formation rates (SFRs) in clusters (see e.g. Nulsen, Johnstone & Fabian 1987). This clearly indicates that a source of heating is needed, that will stop the gas from cooling and condensing on to the central cluster galaxy. The main driving mechanism behind this heating is thought to be active galactic nucleus (AGN) activity, a theory which has been supported by a wealth of studies on galaxy clusters (e.g. Bîrzan et al. 2004; Dunn & Fabian 2006; Rafferty et al. 2006; Fabian 2012; McNamara & Nulsen 2012).

Although AGN activity and other heating mechanisms prevent the ICM from cooling catastrophically, recent observations of brightest cluster galaxies (BCGs) have indicated that the ICM is cooling, albeit at a suppressed rate. In fact, these BCGs seem to possess significant amounts of cold gas, a small part of which is in the process of star formation (Johnstone, Fabian & Nulsen 1987; Allen 1995; O'Dea et al. 2008, 2010). In addition, many CC clusters exhibit optical line filaments, e.g. Abell 1795 (Crawford et al. 2005). It is therefore clear that gas exists in several different phases across a wide temperature range, from the cluster virial temperature (10^7–10^8 K), down to the temperature of molecular clouds (∼10 K), where most of the cold mass in clusters resides (Edge 2001).

In this paper, we study NGC 4696, the BCG of the Centaurus galaxy cluster. NGC 4696 has a redshift of 0.0114 (Struble & Rood 1999), and has been studied extensively, in all wavelengths, because of its proximity (Fabian et al. 1982; Lucey, Currie & Dickens 1986; de Jong et al. 1990; Allen & Fabian 1994; Sanders & Fabian 2002, 2006b; Crawford et al. 2005; Johnstone et al. 2007; Sanders et al. 2008; Canning et al. 2011b; Mittal et al. 2011). Centaurus is a textbook example of a CC cluster, hosting a relatively weak cooling

★ E-mail: caillean@ast.cam.ac.uk

flow of a few tens of $M_\odot\ yr^{-1}$ (e.g. Allen et al. 2001), and having a central cooling time of <0.5 Gyr. A cool-temperature component, at ∼1 keV, in addition to a hotter ∼4 keV component, was first detected by *ASCA* (Fukazawa et al. 1994) and *ROSAT* (Allen & Fabian 1994). The two-temperature model for the ICM was later on confirmed by Allen et al. (2001) and Molendi, De Grandi & Guainazzi (2002). Deep *Chandra* images have revealed a bright core, as well as a plume of gas at the centre of the cluster, extending to the north (Sanders & Fabian 2002). Sanders & Fabian (2002) also showed that the temperature structure of Centaurus is bimodal, with a lower temperature towards the cluster core, and asymmetric in the east–west direction. Both *Chandra* and *XMM–Newton* observations have revealed that the Centaurus cluster has a complex metallicity structure, with steep abundance peaks towards the centre (Sanders & Fabian 2002; Sanders et al. 2008). Using data from the Reflection Grating Spectrometer (RGS) on board *XMM–Newton*, Sanders et al. (2008) find that cooling through X-ray emission below 0.8 keV falls to $<4\,M_\odot\ yr^{-1}$. Sanders & Fabian (2006b) reported enrichment of the ICM gas by a combination of Type Ia supernova (SNIa) and Type II supernova (SNII). Using *Chandra* data, the same authors report a drop in the iron abundance in the central 10 kpc of the Centaurus cluster.

In the optical, Centaurus displays a series of bright line-emitting filaments (Fabian et al. 1982; Crawford et al. 2005), which match the X-ray structure of the cluster, as well as a deep dust lane (Crawford et al. 2005). Using *Herschel*, Mittal et al. (2011) detected cold (∼19 K) and warm (∼46 K) dust emission, with the cold dust component being 400 times more massive than the warm dust component. The same authors also calculated an SFR of $0.13\,M_\odot\ yr^{-1}$. *Spitzer* observations detected emission from NGC 4696 in the near-, mid- and far-infrared, which originates from polycyclic aromatic hydrocarbons, circumstellar dust emission and interstellar dust, respectively (Kaneda, Onaka & Sakon 2005; Kaneda et al. 2007).

Member galaxies of CC clusters are expected to enrich their surrounding gas with metals from SNe and galactic winds. However, the Centaurus cluster is just one of a number of clusters exhibiting a central abundance drop. Other clusters with central abundance dips include Abell 2199 (Johnstone et al. 2002), Abell 1644 (Kirkpatrick et al. 2009) and the Perseus cluster (Schmidt, Fabian & Sanders 2002; Churazov et al. 2003; Sanders et al. 2004). Central abundance dips are also not limited to clusters. Rafferty et al. (2013) report a central abundance drop in the centre of HCG 62, from $\sim 0.8\,Z_\odot$ at a radius of 15 arcsec to $0.3\,Z_\odot$ in the central 5 arcsec. Rasmussen & Ponman (2007) derived iron abundance profiles for 15 Hickson compact groups, showing a dip in the iron abundance in the very centre of most of the groups with a sufficiently resolved core. One of the suggested causes of these abundance dips is resonance scattering (Gilfanov, Syunyaev & Churazov 1987; Sanders & Fabian 2006a). According to this theory, if a galaxy cluster is sufficiently optically thick at the energies of strong resonance lines, radiation that would have otherwise travelled along the line of sight of an observer is now scattered away from that line of sight. If multiple scattering occurs, photons may even be absorbed by cold gas. As a result, the abundance in the centre of the cluster could be underestimated, while the abundance towards the outer regions could be overestimated. However, Sanders & Fabian (2006a) found that resonance scattering does not explain the central abundance dip in Centaurus, although they indicate that internal absorption has a significant effect in the innermost 40 kpc of the cluster.

In this paper, we adopt the cosmology $H_0 = 70$ km s^{-1} Mpc^{-1}, $\Omega_m = 0.27$ and $\Omega_\Lambda = 0.73$. All abundances presented in this paper are relative to solar, as defined in Anders & Grevesse (1989).

2 OBSERVATIONS AND DATA PREPARATION

In our analysis, we used the archival *Chandra* data sets with observation IDs 4954, 4955, 504 and 5310. In all these observations, the Centaurus cluster was placed on the back-illuminated S3 chip of the Advanced CCD Imaging Spectrometer (ACIS) S detector. The data sets were reprocessed using the CIAO ACIS_REPROCESS_EVENTS pipeline, and the appropriate charge transfer inefficiency correction files and gain files were applied to calibrate the data. Each data set was individually examined, in order to excise periods of background flaring. To achieve this, 2.5–7.0 keV light curves were extracted from the back-illuminated S1 chip of the ACIS-S detector. These were then visually examined for periods of background flaring, which were excluded from any subsequent analysis. This process yielded a total exposure time of 198 ks. After the light-curve filtering, each data set was reprojected on to data set 4954.

Blank-sky observations were selected and adjusted to match the individual observations. To account for the increase in background with time in the background observations, their exposure times were altered so that their count rate in the 9.0–12.0 keV energy band matched that of the corresponding cluster observation. The background data sets were then also reprojected on to data set 4954. For the creation of the total background image, the exposure time of each reprojected background image was weighted by the ratio of the cluster observation exposure time over the total exposure time (198 ks). The individual weighted, reprojected background images were then added together to create a total background image.

A 0.5–7.0 keV background-subtracted, exposure-corrected composite image of the Centaurus cluster was created and is shown in Fig. 1. The CIAO WAVDETECT routine was used to identify point sources in this image. The point sources were then visually verified and excluded from all subsequent spectral analysis.

3 SPECTRAL ANALYSIS AND RESULTS

3.1 Analysis

The main aim of our analysis is to study the radial profiles of the cluster temperature, metallicity and enclosed mass. To this end, we extracted spectra from concentric annular regions, centred on the core of the cluster, which we define as the centre of the X-ray emission peak (RA $12^h48^m48\overset{s}{.}8$, Dec. $-41^\circ18'45\overset{''}{.}0$). The annular regions were created in such a way that they all contained the same number of counts, i.e. they all had the same signal-to-noise ratio. The total background-subtracted, but not exposure-corrected cluster image was used to define the annular regions, to ensure that the extracted spectra represented the same region in all the data sets.

We created 22 annuli from the total background-subtracted cluster image, each one containing 115 000 ± 5000 counts in the 0.5–7.0 keV band, corresponding to a signal-to-noise ratio of ∼340. These annuli cover 0.11–70.05 kpc in radius from the defined cluster centre. We extracted foreground spectra and the corresponding background spectra, for each annulus from each of the four data sets. Corresponding ancillary region files and response matrix files were created using MKWARF and MKACISRMF, respectively. To account for projection effects, the spectra were deprojected using the DSDEPROJ routine, as described in Sanders & Fabian (2007) and Russell, Sanders & Fabian (2008). DSDEPROJ is a model-independent deprojection method, which, under the only assumption of spherical symmetry, removes projected emission in a string of shells. After deprojection, the spectra were binned to have a minimum of 25 counts per spectral bin. The joint spectral fits were performed in

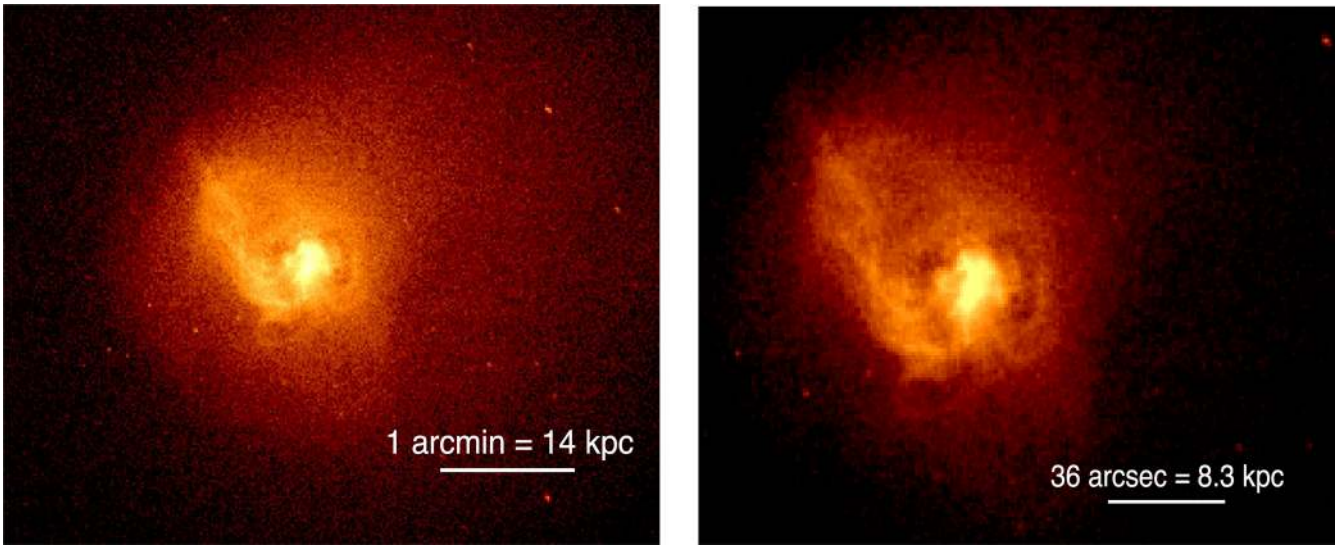

Figure 1. Left: 0.5–7.0 keV composite image of NGC 4696. Two surface brightness edges, one to the west and one closer in to the east of the cluster, are visible. A plume of gas is seen extending to the north, and the two X-ray cavities are clearly visible in this image. North is towards the top of the image and west is to the left. Right: 0.5–7.0 keV composite image of the core of NGC 4696.

XSPEC (Arnaud 1996) v12.7.1b in the 0.5–7.0 keV energy band. The model used for the cluster emission was an absorbed, optically thin, single-temperature thermal plasma model, WABS*VAPEC. The WABS component allows for photoelectric absorption between the cluster and Earth, and the VAPEC term is used to model the thermal emission from the cluster.

The available free parameters in our WABS*VAPEC model are: the column density nH, the temperature, the abundance of He, C, N, O, Ne, Mg, Al, Si, S, Ar, Ca, Fe and Ni, the redshift of the source and the normalization of the thermal VAPEC component. We used a fixed column density of $8.31 \times 10^{20}\,\mathrm{cm}^{-2}$, and a fixed source redshift of 0.0114. We also fixed the He abundance to solar. For each set of four spectra corresponding to the same annular region, we allowed the temperature and iron abundance to vary independently, though their values for the four spectra were tied together. The parameter values of the rest of the abundances were tied to that of iron in the same annulus. To account for the differences in the exposures of the four data sets, the normalization of the VAPEC component was left free to vary, for each of the spectra. We note that, although varying independently, the normalizations for the VAPEC component for the spectra corresponding to the same annulus had very similar values in the resulting spectral fit.

3.2 Results

The spectral fit we performed gave a statistically acceptable fit to the data. The resulting deprojected radial temperature and iron, silicon and sulphur abundance profiles are shown in the left-hand panel of Figs 3 and 2, respectively. The total enclosed mass profile is shown in the right-hand panel of Fig. 3. The temperature profile shows some variability in the 20–45 kpc region. The behaviour in this region is similar to that reported in Sanders & Fabian (2002), where they fit their data with absorbed two-temperature models [WABS*(APEC+APEC)]. The same authors attributed this behaviour to the asymmetry between the temperature profiles in the east and west of the cluster. We note that there are visible surface brightness discontinuities (Fig. 1) at a distance of 16 arcsec to the east and 44.9 arcsec to the west of the cluster centre, consistent with the temperature jumps reported in fig. 9 of Sanders & Fabian (2002)

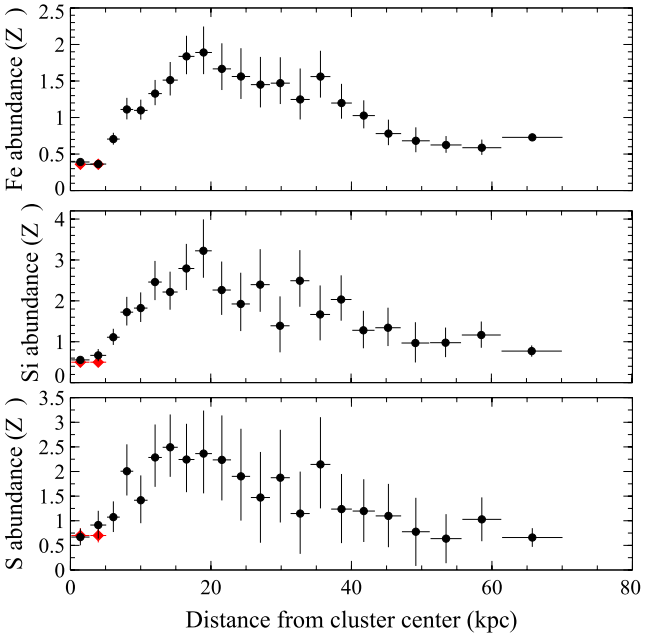

Figure 2. Deprojected iron (top panel), silicon (middle panel) and sulphur (bottom panel) abundance profiles for NGC 4696. The red points denote the best-fitting abundances from the two-temperature fit of the inner two spectral bins. Errors are at the 90 per cent confidence level.

and in Fabian et al. (2005). As we are primarily interested in the iron abundance profile of NGC 4696, we do not investigate the temperature variability in the 20–45 kpc region any further in this paper.

There is an obvious drop in the iron abundance profile within the central 7 kpc of the cluster, as shown in the top panel of Fig. 2. This drop is particularly steep in the innermost 5 kpc. The abundance profile peaks at $1.8\,Z_{\odot}$ at around 20 kpc, and then starts to decline relatively smoothly to $0.6\,Z_{\odot}$ at $\sim$60 kpc. Since we deprojected our spectra before performing the spectral fits, it is unlikely that this central abundance drop is caused by projection effects, and must therefore be real.

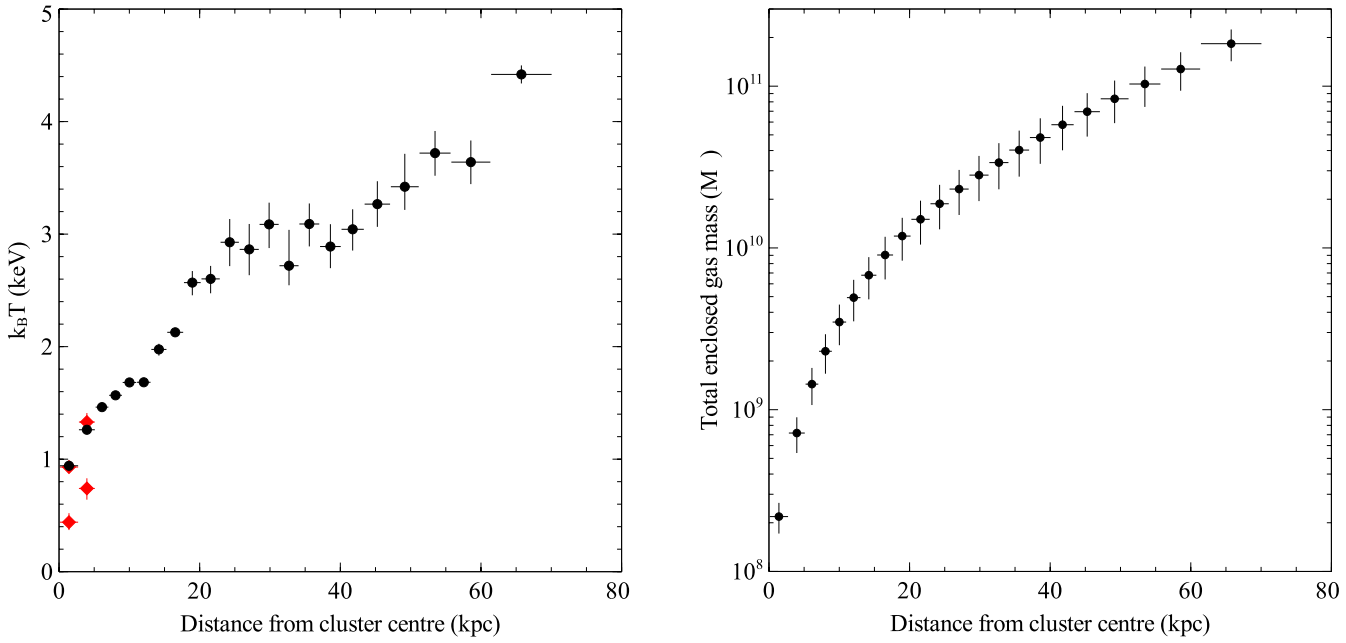

Figure 3. Left: deprojected temperature profile for NGC 4696. The red points denote the best-fitting temperatures from the two-temperature fit of the inner two spectral bins. Right: total enclosed gas mass profile. Errors in all plots are at the 90 per cent confidence level.

3.3 Two-temperature fit for the cluster centre

Previous studies of the Centaurus cluster, using both *XMM–Newton* RGS data (Sanders et al. 2008) and *Chandra* data (Sanders & Fabian 2002), showed that the temperature profile in its innermost regions is bimodal. Based on these findings, to calculate the missing iron mass within 5 kpc, we performed a joint spectral fit of the two innermost spectral bins (which correspond to the inner 5 kpc), using a two-temperature absorbed thermal model, WABS*(VAPEC+VAPEC). In this case, N_H was allowed to vary freely, as were the abundances of O, Ne, Mg, Si, S, Ca, Fe and Ni. The rest of the abundances in the model, namely C, N and Al, were frozen at 0.3 $Z_\odot$, as the energy range of *Chandra* makes the spectra insensitive to C and N. All abundances were tied together for the two-temperature components. For both spectral bins, the temperatures and normalizations for each VAPEC component were left as free parameters, and all the respective abundances were tied. As expected, fitting a two-temperature model to the data, rather than a single-temperature model, significantly improves the quality of the fit. Using the same free parameters, the χ^2/dof decreases from 1384.32/1190 for the single-temperature fit to 1207.87/1187 for the two-temperature fit. The best-fitting values for the parameters of the two-temperature spectral fit are listed in Table 1. The best-fitting temperatures and abundances are shown as red points in the left-hand panel of Figs 3 and 2, respectively.

The abundance ratios of Anders & Grevesse (1989) were used in constructing Fig. 2. The number ratio relative to iron is then 4.68×10^{-5}, so the missing mass of iron within 5 kpc, relative to unit central solar abundance, is 1.4×10^6 $M_\odot$ (i.e. the iron required to increase the present observed abundance from 0.37 to 1 $Z_\odot$).

While the two-temperature model is a much better fit than a single-temperature model for the X-ray emission in the cluster core, it is possible that the temperature structure is even more complex. An additional problem that affects the spectra of the cores of galaxy groups and clusters is the temperature bias (Buote 2001; Werner et al. 2008). This bias has the effect that, when complex structure in cluster cores is modelled using simple single-temperature models, the measured abundances can be biased towards lower values. For these reasons, although the RGS data indicate no third temperature component below 0.4 keV (Sanders et al. 2008), we attempted to model the core emission using a three-temperature model, by adding an extra VAPEC component to our two-temperature model. The normalization and the temperature of this component were allowed to vary freely, while the abundances were tied as in the two-temperature model. We found that adding a third VAPEC component

Table 1. Best-fitting parameter values for joint fit of inner two spectral bins. The errors shown are at the 90 per cent confidence level, and the abundances are relative to solar.

Parameter value		Best-fitting value
1st spectral bin	k$_B$T (keV)	$0.44^{+0.09}_{-0.06}$
	Norm	$(3.52^{+1.28}_{-0.77}) \times 10^{-4}$
	k$_B$T (keV)	0.93 ± 0.02
	Norm	$(1.10^{+0.12}_{-0.10}) \times 10^{-3}$
2nd spectral bin	k$_B$T (keV)	$0.77^{+0.06}_{-0.12}$
	Norm	$(2.64^{+0.67}_{-0.82}) \times 10^{-4}$
	k$_B$T (keV)	$1.35^{+0.08}_{-0.06}$
	Norm	$(8.56^{+1.37}_{-0.95}) \times 10^{-4}$
O		$0.12^{+0.08}_{-0.07}$
Ne		0.38 ± 0.22
Mg		$0.46^{+0.13}_{-0.11}$
Si		$0.54^{+0.08}_{-0.07}$
S		$0.76^{+0.15}_{-0.14}$
Ca, Ar		$1.24^{+0.58}_{-0.56}$
Fe		$0.37^{+0.06}_{-0.05}$
Ni		$1.60^{+0.54}_{-0.50}$
N_H		$15.22^{+1.86}_{-1.93}$ ($\times 10^{20}$ cm^{-2})
χ^2/dof		1207.87/1187 ($\simeq$1.02)

did not significantly improve the fit to the data; the statistical improvement to the fit was relatively small (χ^2/dof = 1198.89/1183). In addition, it was not possible to constrain the value of the temperature of the third component, and the lower limit on its normalization was consistent with zero. However, we note that, even with the three-temperature model, the measured iron abundance remains low at $0.39\,Z_\odot$.

In addition to the two-temperature VAPEC model, we fitted the spectra from the central 5 kpc with a combined single-temperature and cooling flow model, namely WABS*(VAPEC+VMCFLOW). In a cooling flow model (for a review, see Fabian 1994), the gas in galaxy groups and clusters is assumed to be radiatively cooling from an upper temperature to a lower one. For this spectral model, the high-temperature value of the VMCFLOW component was tied to the temperature of the VAPEC component, and the abundances of the two components were tied. The Na abundance of the VMCFLOW component was tied to that of Fe, and the value of its low-temperature component was allowed to vary freely. To prevent the attenuation of unphysically low values, the Ne abundance was tied to that of Fe, while the rest of the abundances were tied as in the WABS*(VAPEC+VAPEC) model. This model was only a slightly worse fit statistically to the data than the two-temperature model, giving χ^2/dof = 1219.59/1188 $\simeq$ 1.03. The measured Fe abundance remains low at $0.44\,Z_\odot$, while the high- and low-temperature components were found to have values equal to 1.12 and 0.38 keV for the innermost bin, and 1.43 and 0.31 keV for the second innermost bin, respectively.

As a final check, we show the radial abundance profiles of silicon and sulphur (middle and bottom panels of Fig. 2, respectively), which are less susceptible to the effect of low-temperature components. The profiles of silicon and sulphur are similar to that of iron. We conclude that the abundance drops observed towards the centre of NGC 4696 are real. We also attempted to determine the radial abundance profiles of other elements, such as argon. Unfortunately, the abundance profiles were highly variable, and could not be physically interpreted.

The two-temperature model of the extended emission from the central 5 kpc of NGC 4696 is a significant improvement over the single-temperature model, and a three-temperature model does not improve the spectral fit. Therefore, our results obtained using a two-temperature model for the core emission are relatively unaffected by projection effects, and the aforementioned temperature bias.

4 WHERE IS THE MISSING IRON?

We now assume that the observed iron abundance drop at the centre of the Centaurus cluster is due to a real absence of iron, and explore where it might be, or has gone. In this section, we compare the missing iron mass with the masses of hot and cold gas, and the dust within the inner 5 kpc of NGC 4696.

A radius of 5 kpc encompasses most of the optical filamentation seen in the galaxy (Fabian et al. 1982; Sparks, Macchetto & Golombek 1989; Crawford et al. 2005; Farage et al. 2010; Canning et al. 2011b), as well as the dust emission (Kaneda et al. 2005, 2007; Mittal et al. 2011) and far-infrared emission from gas (Mittal et al. 2011). The region is clearly multiphase with gas and dust at less than 30 K, warm gas at 10^3–10^4 K, as well as the X-ray emitting gas around 10^7 K. The Hα luminosity is about 2×10^{40} erg s^{-1} (Farage et al. 2010; Canning et al. 2011b), which implies a mass of warm gas of $4 \times 10^5\,M_\odot$ (Farage et al. 2010). The mass of cold gas estimated through its C II emission is 0.5–5 $\times 10^7\,M_\odot$, and the mass of cold dust at about 19 K is $1.6 \pm 0.3 \times 10^6\,M_\odot$ (Mittal et al. 2011).

Iron is usually depleted on to grains in cold gas (see e.g. Draine 2009), and if we assume solar abundance for that gas, then iron will be about 20 per cent of its mass, or about $3.2 \pm 0.6 \times 10^5\,M_\odot$ of iron in grains. The iron abundance of the cold gas could be higher than for the hot gas, so a significant fraction of the missing iron could be in the grains (see also Canning et al. 2011a). Feedback activity caused by the nucleus of the galaxy is demonstrated by the bubbles of radio-emitting plasma evident in Fig. 1, which also lie within the inner 5 kpc. The bubbles are buoyant in the intracluster gas, and will rise, dragging the filamentation outward, as discussed for these and other cluster filaments (Fabian et al. 2003; Crawford et al. 2005). This means that grains are transported outward by the quasi-continuous bubbling process necessary to prevent a full cooling flow developing in the cluster core (for a review, see Fabian 2012). If filaments and grains are somehow destroyed beyond 10–20 kpc, e.g. by sputtering in hot gas, then iron will be returned to the hot medium there, contributing to its high iron abundance (see the top panel of Fig. 2). Silicon can also be depleted on to grains, and possibly sulphur too (see section 2.3 in Calura et al. 2009, and references therein), so explaining their low central abundance values.

An alternative way a central abundance drop can arise is if the iron injected by SNeIa remains clumped, rather than mixing with the surrounding gas. High metallicity gas clumps cool radiatively on a relatively short time-scale, giving much weaker overall iron emission. This is because, while in a high metallicity gas clump the iron ions only have to cool themselves, if they are dispersed in a low metallicity gas cloud, they have to cool the surrounding hydrogen, helium, etc., as well as themselves. This requires the iron emission to be stronger (see Fabian et al. 2001; Morris & Fabian 2003). A problem that arises when trying to apply this solution to the Centaurus cluster is that the abundance drop would not be expected to coincide so well with the dust extent; rather, it would lead to a more extended drop. Nevertheless, this mechanism could play a lesser role in shaping the overall iron abundance profile.

The inner multiphase medium of NGC 4696 is dominated by stellar mass-loss, including ejecta from SNe, and has been modelled by Graham et al. (2006) and Sanders & Fabian (2006b). The fate of stellar mass-loss in central cluster galaxies has been further emphasized by Voit & Donahue (2011). Stellar mass-loss and SNeIa are the sources of iron in the inner region of central cluster galaxies. We estimate the injection of iron from SNIa within the inner 5 kpc to be about $3.4 \times 10^{-3}\,M_\odot\,yr^{-1}$ of iron, using the SN rate given in Pellegrini & Ciotti (2006), a total B-band luminosity of $10^{11}\,L_\odot$ (Sanders & Fabian 2006b) and the Hernquist stellar profile of Farage et al. (2010), according to which 43 per cent of the projected light is contained within a 5 kpc radius. This means that the missing iron corresponds to about 0.4 Gyr of SN injection within 5 kpc. For stellar mass-loss, we obtain an injection rate of $1.3\,M_\odot\,yr^{-1}$ for within 5 kpc, and an iron injection rate (assumed to be at solar abundance) of $3.4 \times 10^{-3}\,M_\odot\,yr^{-1}$, identical to the SNIa rate, using the Pellegrini & Ciotti (2006) rate used by Sanders & Fabian (2006b), assuming an age of 10^{10} yr. Much of that iron can have originated in SNII during the early growth of the galaxy. From abundance ratios, Sanders & Fabian (2006b) find that the main metallicity peak has been enriched 70 per cent by SNIa and 30 per cent by SNII.

Voit & Donahue (2011) suggest that some of the stellar mass-loss remains cool and distinct from the surrounding hot gas, and thus preserves its embedded dust, making the cold filaments dusty. Ultraviolet observations of the stripped wake of the giant star Mira in our galaxy support this hypothesis (Martin et al. 2007). It is thus

possible that much of the iron in the stellar mass-loss remains in grain form, and is incorporated into the filaments. The only hot atomic iron in the inner region is then that due to SNIa.

The particle heating model of Ferland et al. (2009) successfully explains the line ratios of cluster filament systems, such as that around NGC 4696. The surrounding hot gas at temperature $10^7 T_7$ K interpenetrates the filaments and becomes incorporated in them at a rate of $\sim 0.7 L(\mathrm{H}\alpha)_{40} T_7^{-1}\,\mathrm{M}_\odot\,\mathrm{yr}^{-1}$, producing an H$\alpha$ luminosity of $10^{40} L(\mathrm{H}\alpha)_{40}\,\mathrm{erg\,s}^{-1}$. For NGC 4696, this means a rate of about $1.4\,\mathrm{M}_\odot\,\mathrm{yr}^{-1}$, where $T_7 \sim 1$, so that most of the inner gas may be processed in this way in $\sim 5 \times 10^8$ yr.

We note that, if the SNIa-injected iron remains localized, then high iron abundance clumps of hot gas will result. Such clumps can perhaps explain the detection of [Fe X]λ6374 coronal line emission from iron (Canning et al. 2011a). These clumps can cool rapidly, triggering iron-rich cold clouds (Fabian et al. 2001; Morris & Fabian 2003). The cold iron can then grow on to grains.

The low measured oxygen abundance in the central 5 kpc (see Table 1) is explained if we assume that most oxygen is also in cold dust grains. SNIa produce a negligible amount of oxygen, compared to iron, so that the hot gas naturally has a low central oxygen abundance. This result can also help explain the weakness of O VII emission seen in CC clusters (Sanders & Fabian 2011). The appearance, abundances and quantities of gas at temperatures of 10^6–10^7 K in this environment are very complicated.

We assume, then, that there is a quasi-continuous cyclical process of bubbling, which leads to the dusty clouds being eventually dragged away from the centre. The age of the present bubbles is $\sim 6 \times 10^6$ yr (Dunn & Fabian 2006), and the time for each cycle could be slightly longer, at 10^7 yr. At the above present SNII iron injection rate, it takes 9.4×10^7 yr to accumulate the level of iron inferred from the observed mass of dust. Thus, an approximate steady state is reached if about 10 per cent of the filaments, with their embedded grains, is dragged out from the central 5 kpc in each cycle. Some of the SNIa enriched hot gas will also be dragged outward.

5 DISCUSSION

The drop in iron abundance observed within the central few kpc of the Centaurus cluster is plausibly due to the iron injected by stellar mass-loss remaining bound in dust grains, as proposed by Voit & Donahue (2011). The missing iron is then in the grains, seen at optical and far-infrared wavelengths in the dusty filaments occupying the same spatial region as the abundance drop, and at larger radii in both cold and hot gas where it has been transported by the bubbling process of feedback in the cluster core. Grains provide a plausible method for separating iron and other refractory metals from hydrogen, so leading to large central abundance drops.

Further work on the scenario outlined here requires further observations of the detailed metallicity of the stars and cold gas in NGC 4696, as well as of the hot gas. Deeper *Chandra* observations, in particular, are needed. The inner region of NGC 4696, at the centre of the Centaurus cluster, is a unique nearby environment for studying stellar mass-loss in giant elliptical galaxies.

ACKNOWLEDGEMENTS

We thank Raymond Oonk for helpful discussions. EKP acknowledges the support of a STFC sudentship. ACF thanks the Royal Society for support. We would like to thank the anonymous referee for helpful comments that improved the content of this paper.

The plots in this paper were created using VEUSZ.[1]

REFERENCES

Allen S. W., 1995, MNRAS, 276, 947
Allen S. W., Fabian A. C., 1994, MNRAS, 269, 409
Allen S. W., Fabian A. C., Johnstone R. M., Arnaud K. A., Nulsen P. E. J., 2001, MNRAS, 322, 589
Anders E., Grevesse N., 1989, Geochim. Cosmochim. Acta, 53, 197
Arnaud K. A., 1996, in Jacoby G. H., Barnes J., eds, ASP Conf. Ser. Vol. 101, XSPEC: The First Ten Years. Astron. Soc. Pac., San Francisco, p. 17
Bîrzan L., Rafferty D. A., McNamara B. R., Wise M. W., Nulsen P. E. J., 2004, ApJ, 607, 800
Buote D. A., 2001, ApJ, 548, 652
Calura F., Dessauges-Zavadski M., Prochaska J. X., Matteucci F., 2009, ApJ, 693, 1236
Canning R. E. A., Fabian A. C., Johnstone R. M., Sanders J. S., Crawford C. S., Hatch N. A., Ferland G. J., 2011a, MNRAS, 411, 411
Canning R. E. A., Fabian A. C., Johnstone R. M., Sanders J. S., Crawford C. S., Ferland G. J., Hatch N. A., 2011b, MNRAS, 417, 3080
Churazov E., Forman W., Jones C., Böhringer H., 2003, ApJ, 590, 225
Crawford C. S., Hatch N. A., Fabian A. C., Sanders J. S., 2005, MNRAS, 363, 216
de Jong T., Norgaard-Nielsen H. U., Jorgensen H. E., Hansen L., 1990, A&A, 232, 317
de Plaa J., Werner N., Bleeker J. A. M., Vink J., Kaastra J. S., Méndez M., 2007, A&A, 465, 345
Draine B. T., 2009, in Henning T., Grün E., Steinacker J., eds, ASP Conf. Ser. Vol. 414, Interstellar Dust Models and Evolutionary Implications. Astron. Soc. Pac., San Francisco, p. 453
Dunn R. J. H., Fabian A. C., 2006, MNRAS, 373, 959
Edge A. C., 2001, MNRAS, 328, 762
Edge A. C., Stewart G. C., 1991, MNRAS, 252, 414
Fabian A. C., 1994, ARA&A, 32, 277
Fabian A. C., 2012, ARA&A, 50, 455
Fabian A. C., Nulsen P. E. J., Atherton P. D., Taylor K., 1982, MNRAS, 201, 17P
Fabian A. C., Mushotzky R. F., Nulsen P. E. J., Peterson J. R., 2001, MNRAS, 321, L20
Fabian A. C., Sanders J. S., Crawford C. S., Conselice C. J., Gallagher J. S., Wyse R. F. G., 2003, MNRAS, 344, L48
Fabian A. C., Sanders J. S., Taylor G. B., Allen S. W., 2005, MNRAS, 360, L20
Farage C. L., McGregor P. J., Dopita M. A., Bicknell G. V., 2010, ApJ, 724, 267
Ferland G. J., Fabian A. C., Hatch N. A., Johnstone R. M., Porter R. L., van Hoof P. A. M., Williams R. J. R., 2009, MNRAS, 392, 1475
Finoguenov A., David L. P., Ponman T. J., 2000, ApJ, 544, 188
Fukazawa Y., Ohashi T., Fabian A. C., Canizares C. R., Ikebe Y., Makishima K., Mushotzky R. F., Yamashita K., 1994, PASJ, 46, L55
Gilfanov M. R., Syunyaev R. A., Churazov E. M., 1987, Sov. Astron. Lett., 13, 3
Graham J., Fabian A. C., Sanders J. S., Morris R. G., 2006, MNRAS, 368, 1369
Johnstone R. M., Fabian A. C., Nulsen P. E. J., 1987, MNRAS, 224, 75
Johnstone R. M., Allen S. W., Fabian A. C., Sanders J. S., 2002, MNRAS, 336, 299
Johnstone R. M., Hatch N. A., Ferland G. J., Fabian A. C., Crawford C. S., Wilman R. J., 2007, MNRAS, 382, 1246
Kaneda H., Onaka T., Sakon I., 2005, ApJ, 632, L83
Kaneda H., Onaka T., Kitayama T., Okada Y., Sakon I., 2007, PASJ, 59, 107

[1] http://home.gna.org/veusz/

Kirkpatrick C. C. et al., 2009, ApJ, 697, 867
Loewenstein M., 2006, ApJ, 648, 230
Lucey J. R., Currie M. J., Dickens R. J., 1986, MNRAS, 221, 453
Martin D. C. et al., 2007, Nat, 448, 780
McNamara B. R., Nulsen P. E. J., 2007, ARA&A, 45, 117
McNamara B. R., Nulsen P. E. J., 2012, New J. Phys., 14, 055023
Mittal R. et al., 2011, MNRAS, 418, 2386
Molendi S., De Grandi S., Guainazzi M., 2002, A&A, 392, 13
Morris R. G., Fabian A. C., 2003, MNRAS, 338, 824
Nulsen P. E. J., Johnstone R. M., Fabian A. C., 1987, Proc. Astron. Soc. Aust., 7, 132
O'Dea C. P. et al., 2008, ApJ, 681, 1035
O'Dea K. P. et al., 2010, ApJ, 719, 1619
Pellegrini S., Ciotti L., 2006, MNRAS, 370, 1797
Peterson J. R., Fabian A. C., 2006, Phys. Rep., 427, 1
Rafferty D. A., McNamara B. R., Nulsen P. E. J., Wise M. W., 2006, ApJ, 652, 216
Rafferty D. A., Bîrzan L., Nulsen P. E. J., McNamara B. R., Brandt W. N., Wise M. W., Röttgering H. J. A., 2013, MNRAS, 428, 58
Rasmussen J., Ponman T. J., 2007, MNRAS, 380, 1554
Russell H. R., Sanders J. S., Fabian A. C., 2008, MNRAS, 390, 1207
Sanders J. S., Fabian A. C., 2002, MNRAS, 331, 273
Sanders J. S., Fabian A. C., 2006a, MNRAS, 370, 63
Sanders J. S., Fabian A. C., 2006b, MNRAS, 371, 1483
Sanders J. S., Fabian A. C., 2007, MNRAS, 381, 1381
Sanders J. S., Fabian A. C., 2011, MNRAS, 412, L35
Sanders J. S., Fabian A. C., Allen S. W., Schmidt R. W., 2004, MNRAS, 349, 952
Sanders J. S., Fabian A. C., Allen S. W., Morris R. G., Graham J., Johnstone R. M., 2008, MNRAS, 385, 1186
Schmidt R. W., Fabian A. C., Sanders J. S., 2002, MNRAS, 337, 71
Sparks W. B., Macchetto F., Golombek D., 1989, ApJ, 345, 153
Struble M. F., Rood H. J., 1999, ApJS, 125, 35
Voit G. M., Donahue M., 2011, ApJ, 738, L24
Werner N., Durret F., Ohashi T., Schindler S., Wiersma R. P. C., 2008, Space Sci. Rev., 134, 337

This paper has been typeset from a TEX/LATEX file prepared by the author.